# Identification of frame dynamics of vertically oriented high-speed steam generator using model update procedure for reduced-order model

Sikanen Eerik, Heikkinen Janne, Sillanpää Teemu, Scherman Eero, Sopanen Jussi



**DOI:** 10.1201/9781003132639-38

*12th International Conference on Vibrations in Rotating Machinery - Institution of Mechanical Engineers, ISBN 978-0-367-67742-8*

# Identification of frame dynamics of vertically oriented high-speed steam generator using model update procedure for reduced-order model

**E. Sikanen[1], J. Heikkinen[1], T. Sillanpää[1], E. Scherman[2], J. Sopanen[1]**

[1]Lappeenranta-Lahti University of Technology, Lappeenranta, Finland
[2]Saimaa University of Applied Sciences, Lappeenranta, Finland

## ABSTRACT

Active Magnetic Bearing (AMB) systems are common in high-speed rotating machinery. Bearing control system input is the relative displacement data measured between the sensor and the measurement surface. In case of frame resonance, controller may create a feedback loop which may amplify the frame vibration modes. The frame vibration dynamics of 1 MW steam generator with AMB-support is studied. Vibration mode identification using FE-based model are discussed. Model-order reduction techniques are utilized to solve a large-scale numerical problem. The paper shows an update procedure for a computationally efficient reduced-order model that can be used for identifying measured unclear vibration modes.

## 1 INTRODUCTION

Active Magnetic Bearing (AMB) systems are often considered as the most suitable bearing solution for rotating high-speed applications. As the AMB system utilize active feedback control, the quality of the position signal is essential for the stability of the bearing control system. In AMB systems, rotor position signal is measured between the stator frame and the rotor lamination yielding a relative displacement. In cases where frame dynamics significantly contributes to system dynamics, the relative displacement of AMB sensor should not be considered as absolute reading since in worst case it can cause amplified vibration due to a possible feedback loop in the conventional AMB control system [1]. Often, as the power rating of the high-speed machines increase, the size and mass of the machine structure is increased, and thus, the need of analysing the frame dynamics becomes more important. Electrical machine frame vibration dynamics with magnetically suspended rotor seems to be a topic not often discussed in literature.

The finite element method (FEM) is often used for solving numerical vibration problems. The use of three-dimensional (3D) solid element models is nowadays a standard practice. Often, due to fine discretization of the structure, the problem size may become very large, thus causing very long computation times in solution. Therefore, model-order reduction becomes necessary. Vibration analysis in modal domain has its own requirements compared to time domain analysis in which contacts and constraints may be expressed simply as time-dependent forces at boundaries. In modal domain, individual components are required have physical boundary degrees-of-freedom for body-to-body coupling to be utilized. The concept of superelement-based techniques is well known, and perhaps the most well-known method utilized is the Craig-Bampton method [2]. When using substructuring [3] and modelling individual subdomains as single superelements, a very large problem can be reduced significantly without losing much accuracy [4]. Although, there are multiple model-order reduction methods [5] available, such as System Equivalent Reduction Expansion

Process (SEREP) [6] and Improved Reduced System (IRS) [7], the Craig-Bampton method has advantages as the superelement can have variable boundary constraints, and thus, assembling of multiple superelements is enabled. Generating and assembling superelements is possible in commercial FE-software, but the model update options for reduced-order model seems to be very limited [8].

As a case example, the frame dynamics of vertically oriented steam generator is investigated. In the case example, a harmful frame resonance was detected at operating speed range during the AMB commissioning. The problematic frame resonance frequency was identified with both axial and radial AMB sensors, but the mode of this frequency was still unknown. FEM was utilized for modelling the complete generator assembly. In order capture the machine dynamics properly the mesh have to be dense. As a result, the size of finite element (FE) problem became too large to be solved within reasonable time. Thus, model-order reduction techniques were utilized. Substructuring was utilized in order to generate submodels for the Craig-Bampton transformation. The generated superelements were assembled and eigenvectors were solved, and then expanded into global degrees-of-freedom in order to visualize the vibration modes. The problematic frame vibration mode was then identified.

In addition, the suspected axial-radial coupling of the vibration mode was studied using harmonic response analysis. For this analysis, a reduced-order model update procedure is proposed. The model update referred here is modal-based update for dynamic problems in modal domain focusing on eigenmode frequency and corresponding modal damping ratio updates. A customizable 3D solid FEM-based code implemented in MATLAB environment is utilized for the modelling and solving of eigenproblem with multiple superelements [9]. The main reason for using in-house made FEM code arises from the need of fully customizable solver programming in order to make all steps required, generation of superelements, assembly and model update, in the same modelling environment. As result, the proof of existence of the suspected axial-radial vibration coupling in the case study was revealed based on the model update procedure proposed in this work.

## 2 SUBSTRUCTURING AND REDUCED-ORDER MODEL UPDATE

Basic idea of substructuring is to divide the large model into several submodels. Every submodel is transformed into an arbitrary shaped element, generally called as superelement, having a number of selected boundary degrees-of-freedom. Common method for generating a superelement is the Craig-Bampton transformation. Craig-Bampton method produces physical boundary degrees-of-freedom, thus, allowing superelement to be connected with other elements. Craig-Bampton transformation allows full expansion of the reduced-order solution. Thus, it is ideal method for studying large complex-shaped structures in frequency domain. Still, updating dynamic properties of individual submodel is not directly possible due to the characteristics of Craig-Bampton method. Assembled superelement-based reduced-order model can be updated after modal decoupling.

### 2.1 Craig-Bampton method

Due to the large size of the vibration problem discussed in this work, substructuring of a full FE-model is utilized. Craig-Bampton method is used for generating superelements. The Craig-Bampton transformation matrix for generating a superelement can be written as follows [2]:

$$\mathbf{T}_{\mathrm{CB}} = \begin{bmatrix} \boldsymbol{\Phi}_{ik} & \boldsymbol{\Psi}_{ib} \\ \mathbf{0} & \mathbf{I}_{bb} \end{bmatrix} \tag{1}$$

where $\boldsymbol{\Psi}_{ib}$ is the coupling matrix between the internal and boundary degrees of freedom, which can be written as follows:

$$\boldsymbol{\Psi}_{ib} = -\mathbf{K}_{ii}^{-1}\mathbf{K}_{ib} \tag{2}$$

and $\boldsymbol{\Phi}_{ik}$ is the matrix containing a subset of eigenvectors as follows:

$$\boldsymbol{\Phi}_{ik} = \left[\boldsymbol{\Phi}_{i1}\boldsymbol{\Phi}_{i2}\ldots\boldsymbol{\Phi}_{ik}\right] \tag{3}$$

The eigenvectors used for making Craig-Bampton transformation can be solved as follows:

$$(\mathbf{K}_{ii} - \lambda_n\mathbf{M}_{ii})\boldsymbol{\Phi}_n = 0 \tag{4}$$

Using an elastic stiffness matrix as an example, the structural matrices shall be re-arranged for the Craig-Bampton transformation as follows:

$$\mathbf{T}_R^{\mathrm{T}}\mathbf{K}^e\mathbf{T}_R = \mathbf{K}_R^e = \begin{bmatrix} \mathbf{K}_{ii} & \mathbf{K}_{ib} \\ \mathbf{K}_{bi} & \mathbf{K}_{bb} \end{bmatrix} \tag{5}$$

where $\mathbf{T}_R$ is the transformation matrix for matrix reordering, $\mathbf{K}^e$ is the original elastic stiffness matrix and $\mathbf{K}_R^e$ is the re-arranged elastic stiffness matrix derived for purpose of generating a superelement.

Using an elastic stiffness matrix as an example, the Craig-Bampton transformation is completed and deriving a superelement can be written as follows:

$$\mathbf{K}_{\mathrm{CB}}^e = \mathbf{T}_{\mathrm{CB}}^{\mathrm{T}}\mathbf{K}_R^e\mathbf{T}_{\mathrm{CB}} \tag{6}$$

### 2.2 Expanding eigenvalue solution

The reduced-order eigenvalue problem is solved based on assembled FE-model made of individual superelements. Using the Craig-Bampton transformation, the reduced-order solution can be expanded into original size as follows:

$$\boldsymbol{\Phi}_{n,G} = \mathbf{T}_R\left(\mathbf{T}_{\mathrm{CB},k}\boldsymbol{\Phi}_{n,k}\right) \tag{7}$$

where the subscripts *k* and *G* indicates the index of superelement and the expanded original global order of the degrees-of-freedom, respectively.

### 2.3 Assembly of superlements

Assuming a typical rotating machine construction consisting three main parts: support, frame and rotor, the assembled equations of motion can be written as follows:

$$\begin{bmatrix} \mathbf{M}_{\mathrm{CB},S} & \mathbf{0} & \mathbf{0} \\ \mathbf{0} & \mathbf{M}_{\mathrm{CB},F} & \mathbf{0} \\ 0 & 0 & \mathbf{M}_{\mathrm{CB},R} \end{bmatrix} \begin{bmatrix} \ddot{\mathbf{x}}_S \\ \ddot{\mathbf{x}}_F \\ \ddot{\mathbf{x}}_R \end{bmatrix} + \begin{bmatrix} \mathbf{C}_{\mathrm{CB},S} + \mathbf{C}_S + \mathbf{C}_c & -\mathbf{C}_c & \mathbf{0} \\ -\mathbf{C}_c & \mathbf{C}_{\mathrm{CB},F} + \mathbf{C}_c + \mathbf{C}_b & -\mathbf{C}_b \\ \mathbf{0} & -\mathbf{C}_b & \mathbf{C}_{\mathrm{CB},R} + \Omega\mathbf{G}_{\mathrm{CB},R} + \mathbf{C}_b \end{bmatrix}$$
$$\begin{bmatrix} \dot{\mathbf{x}}_S \\ \dot{\mathbf{x}}_F \\ \dot{\mathbf{x}}_R \end{bmatrix} + \begin{bmatrix} \mathbf{K}^e_{\mathrm{CB},S} + \mathbf{K}_S + \mathbf{K}_c & -\mathbf{K}_c & \mathbf{0} \\ -\mathbf{K}_c & \mathbf{K}^e_{\mathrm{CB},S} + \mathbf{K}_S + \mathbf{K}_c & -\mathbf{K}_b \\ \mathbf{0} & -\mathbf{K}_b & \mathbf{K}^e_{\mathrm{CB},R} \end{bmatrix} \begin{bmatrix} \mathbf{x}_S \\ \mathbf{x}_F \\ \mathbf{x}_R \end{bmatrix} = \boldsymbol{F} \tag{8}$$

where matrices $\mathbf{M}$, $\mathbf{K}$, $\mathbf{C}$ and $\mathbf{G}$, in general, contribute to mass, stiffness, damping and gyroscopic effects, respectively, the subscripts $\mathrm{CB}$, $S$, $F$ and $R$ contribute to Craig-Bampton transformation, support, frame assembly and rotor, respectively, $\Omega$ is the rotor angular velocity, $\boldsymbol{x}$ is the vector of nodal coordinates and $\mathbf{F}$ is the vector of external forces. The coupling stiffness and damping matrices $\mathbf{K}_S$ and $\mathbf{C}_S$, $\mathbf{K}_c$ and $\mathbf{C}_c$ and $\mathbf{K}_b$ and $\mathbf{C}_b$ contribute to foundation-to-support, support-to-frame and frame-to-rotor couplings.

### 2.4 Assembled model update

FE-model update based on measured dynamic properties becomes straightforward. The eigenfrequency and modal damping ratio can be updated based on measured data to match the corresponding eigenmode. The assembled superelement expression is used as basis. Equation (8) can be rewritten as follows:

$$\mathbf{M}_A\ddot{\boldsymbol{x}}_A + \mathbf{C}_A\dot{\boldsymbol{x}}_A + \mathbf{K}_A\boldsymbol{x}_A = \boldsymbol{F}_A \tag{9}$$

where the subscript $A$ indicates assembled matrices. After solving a subset of lowest undamped eigenvectors of Equation (9) and mass normalizing the eigenvectors, the structural modal coordinate matrices can be written as follows:

$$\begin{aligned} \widetilde{\mathbf{M}} &= \boldsymbol{\Phi}_A^{\mathrm{T}}\mathbf{M}_A\boldsymbol{\Phi}_A \\ \widetilde{\mathbf{K}} &= \boldsymbol{\Phi}_A^{\mathrm{T}}\mathbf{K}_A\boldsymbol{\Phi}_A \\ \widetilde{\mathbf{C}} &= \boldsymbol{\Phi}_A^{\mathrm{T}}\mathbf{C}_A\boldsymbol{\Phi}_A \end{aligned} \tag{10}$$

where $\widetilde{\mathbf{M}}$, $\widetilde{\mathbf{K}}$ and $\widetilde{\mathbf{C}}$ are the modal mass, stiffness and damping matrices, respectively. Updated modal matrices for modal harmonic response analysis can be written as follows:

$$\begin{aligned} \widetilde{\mathbf{M}} &= \mathbf{I} \\ \widetilde{\mathbf{K}} &= \boldsymbol{\omega}^{\mathrm{T}}\boldsymbol{\omega} \\ \widetilde{\mathbf{C}} &= 2\boldsymbol{\omega}\boldsymbol{\xi} \end{aligned} \tag{11}$$

where $\omega$ and $\xi$ are diagonal matrices containing the modal angular frequencies and modal damping ratios, respectively.

The update procedure presented is valid only for updating the eigenfrequency and modal damping ratio of the particular eigenpair, not for updating the eigenmode vector itself. Updating individual eigenvector has certain limitations as the initial selection of the boundary degrees-of-freedom will have influence on the outcome, and thus, the Craig-Bampton transformation must be redone.

### 2.5 Harmonic response

The equation for harmonic problem using modal coordinate expression can be written as follows [10]:

$$\begin{bmatrix} \widetilde{\mathbf{K}} - \omega^2 \widetilde{\mathbf{M}} & -\omega \widetilde{\mathbf{C}} \\ \omega \widetilde{\mathbf{C}} & \widetilde{\mathbf{K}} - \omega^2 \widetilde{\mathbf{M}} \end{bmatrix} \begin{bmatrix} \widetilde{\boldsymbol{p}}_s \\ \widetilde{\boldsymbol{p}}_c \end{bmatrix} = \begin{bmatrix} \boldsymbol{\Phi}_A^{\mathrm{T}} \boldsymbol{F}_{A,s} \\ \boldsymbol{\Phi}_A^{\mathrm{T}} \boldsymbol{F}_{A,c} \end{bmatrix} \tag{12}$$

The physical displacement vector of the assembly $\mathbf{x}_A$ can be written as follows:

$$\boldsymbol{x}_A = \boldsymbol{\Phi}_A (\tilde{\boldsymbol{p}}_s \ sin\theta + \tilde{\boldsymbol{p}}_c \ \cos\theta) \tag{13}$$

## 3 CASE EXAMPLE: HIGH-SPEED STEAM TURBINE

The studied 1 MW 12,500 rpm high-speed turbine-generator construction under investigation is illustrated in Figure 1. Vertical design was selected in order to have less bearing load in radial direction, thus, minimizing the length of radial AMB laminations on the rotor. In addition, rotor has inner water-cooling channels, which were more functional in case of vertically oriented rotor. In the lower end of the frame construction is located the turbine housing, and on the shaft the double-sided four-phase radial steam turbine impeller. The center of mass of the machine is relatively high due to the need for connecting the steam outlet tubing that would be fastened at the bottom of turbine housing.

In order to visualize the problematic frame vibration mode, a complete generator assembly including the full support leg construction was modelled using FEM. Linear time invariant system is assumed. In order to reduce the problem size, undamped eigenvalues are solved. Regardless of the simplifications to the model of the generator assembly, the FE-problem size was too large to be solved without model-order reduction in sufficient time. Therefore, substructuring of full assembly was utilized. The assembly was split into three submodels, and superelements were generated based on every submodel using Craig-Bampton transformation. The details of the connectivity of superelements are discussed. Using reduced-order assembled superelement-based model, the solution of eigenvalue problem was obtained, and the problematic frame vibration was managed to be visualized using reduced-order solution expansion based on the Craig-Bampton transformation. Also, harmonic response analysis was performed in order to study further the possible axial-radial coupling of this frame vibration mode in question. For this response analysis, the reduced-order model dynamical properties were updated using the measured vibration data so that mode frequencies and damping ratios were obtained from the measurement data and updated into the numerical model.

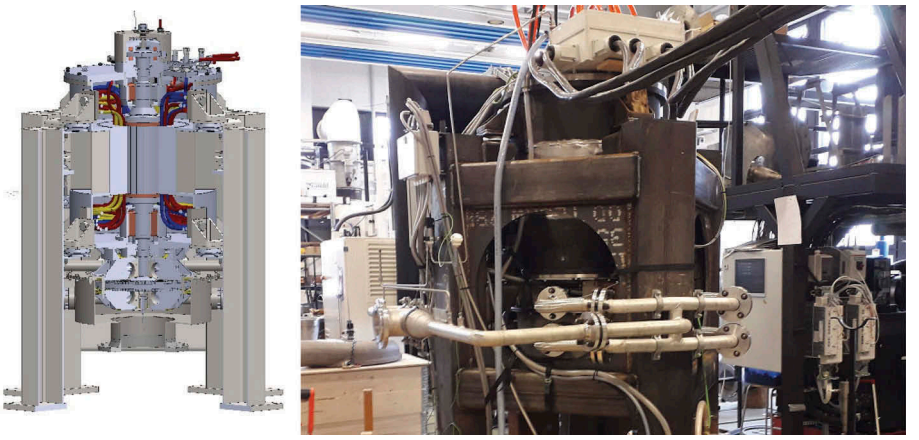

**Figure 1. 1 MW hermetic high-speed steam generator. On the left is the detailed view of the CAD model, and on the right is the fully instrumented generator in laboratory.**

### 3.1 Model substructuring and assembly of superelements

The complete generator assembly illustrated in Figure 1 was divided into three sub-structures: support legs, frame assembly and rotor. These submodels are visualized in Figure 2. The number of degrees-of-freedom of different submodels, and the original and final reduced-order models are given in Table 1. The discretization of individual submodels is made using quadratic tetrahedron elements. The connections between components of a single subassembly are linearized.

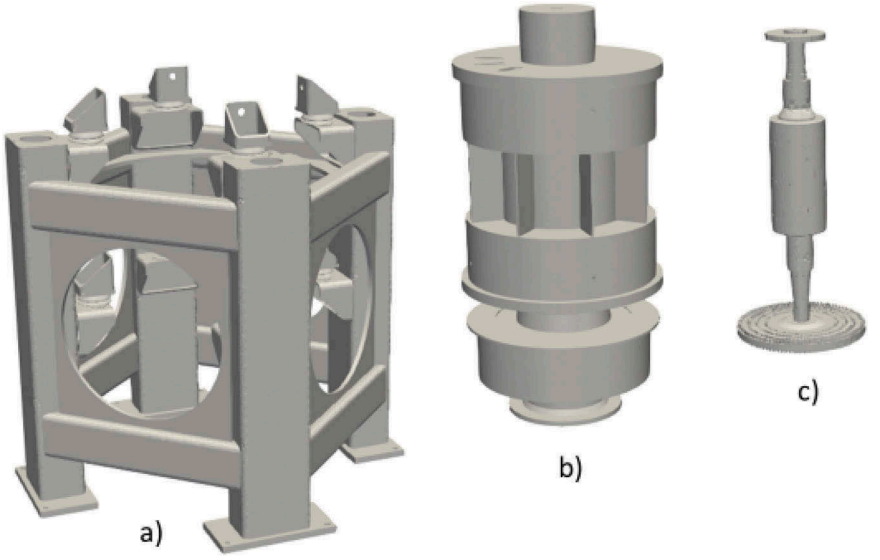


**Figure 2. Three submodels used: a) support legs, b) frame assembly and c) rotor.**

**Table 1. Original and reduced-order model size.**

| Submodel | Original size (dofs) | Superelement size (dofs) |
|---|---|---|
| Support legs | 805,767 | 744 |
| Frame assembly | 765,036 | 684 |
| Rotor | 1,154,202 | 204 |
| Total | 2,725,005 | 1,632 |

The size of individual superelements is based on two factors: the number of flexible modes used and the number of the boundary dofs included into the element. The number of the lowest flexible modes per submodel was set to 24, and the number of nodes per individual connection was set to be approximately 50% of all boundary nodes. The use of reduced number of boundary nodes for contact reduced the size of the transformation matrix effectively without yielding too soft boundary connection. The number of connections is different, in this case, for every submodel as follows:

- Support legs
  - 8 x body-to-ground connections
  - 8 x body-to-body connections between legs and frame
- Frame assembly
  - 8 x body-to-body connections between legs and frame
  - 3 x body-to-body connections between frame and rotor
- Rotor
  - 3 x body-to-body connections between frame and rotor

The leg support body-to-ground connections are assumed to be stiff, thus, the foundation flexibility is neglected in this case. It is reasonable since the body-to-body connections between the support legs and frame are very soft due to installed vibration isolators. Based on identified axial rigid body mode frequency of the frame and the total mass of the frame assembly, the spring stiffness of a single degree-of-freedom mass-point system was calculated, and the equivalent stiffness of a single support-to-frame contact describing single vibration isolator was calculated to be $0.668 \cdot 10^6$ N/m. The body-to-body connections between the frame and rotor are the linearized AMB stiffnesses. In order to obtain accurate values, both radial and axial stiffnesses of the AMB were identified by tuning the model to match the measurements. In radial direction, the model was tuned to match the measured first lateral bending mode of rotor and, as a result, a radial AMB stiffness of $4 \cdot 10^6$ N/m was obtained. Similarly, the axial rigid mode of the rotor was identified based on measurement data, and from the frequency and the mass of the rotor the axial AMB stiffness of $5.16 \cdot 10^6$ N/m was obtained.

### 3.2 Model update for harmonic response analysis

Once the problematic frame vibration mode is identified, the modal reduced FE-model is updated using the method presented in Section 2.4 to match the measured eigenmode frequencies, and the corresponding modal damping ratios are calculated from the measured data. Then, modal harmonic problem is solved, and the coupled axial-lateral mode responses are compared against the measured axial and lateral vibration frequency responses. The solution of the harmonic response is along the inertial coordinate system used, although, the results will be processed so that only relative

displacements between the sensor housings and measurement surfaces are presented.

## 4 RESULTS

The results of the problematic frame vibration mode among the other measured resonances are studied and discussed. The mode of the problematic frame vibration is identified by using both experimental data and the numerical simulation results.

### 4.1 Experimental data

Experimental frequency responses were measured in both axial and radial directions. The data is based on the AMB sensor data, and thus, the nature of the position data recorded is relative. The excitation force is generated using AMBs for system identification purposes for non-rotating machinery. The axial sensor was located in the N-end near the axial bearing. Two radial sensor per lateral axis were used at both radial bearing locations. Logically, the N-end, or ND-end, is the upper end, and the D-end, or drive-end, is the turbine end. The measured data is converted into frequency domain, and the resolution in the axial channel is 0.5 Hz, while in radial channels 1/3 Hz. The frequency responses of one axial and two radial channels are presented and relevant resonance peaks are marked. The modes of these identified frequencies are presented in Table 2. From axial frequency response in Figure 3, it can be seen that in N-end there is a strong resonance at frequency of 117 Hz. This frequency corresponds to the problematic frame vibration. Identification of the other frequencies in the axial frequency response requires the use of FEM-based vibration model.

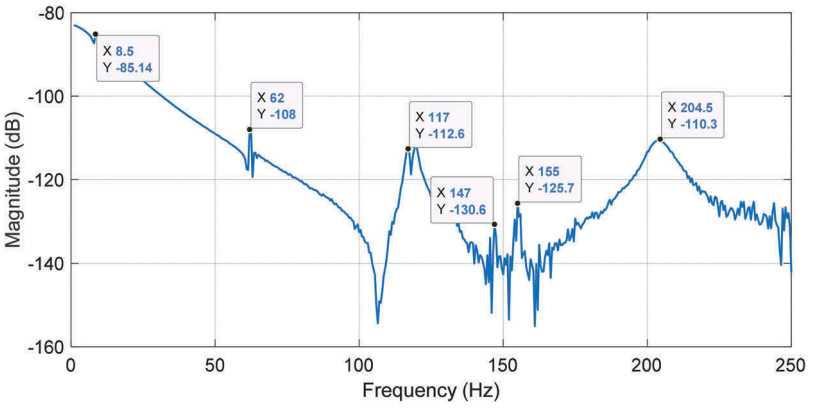


**Figure 3. Measured axial frequency response.**

Previously discussed axial-radial vibration mode coupling is indeed visible in the radial frequency response. In Figure 4, considering the resolution of the plot, the frequency of the coupled axial-radial mode is approximately at 117…118 Hz. Similarly, in the case of axial frequency response, the identification of other modes requires the use of FEM-based vibration model. The modes of these identified frequencies are presented in Table 2.

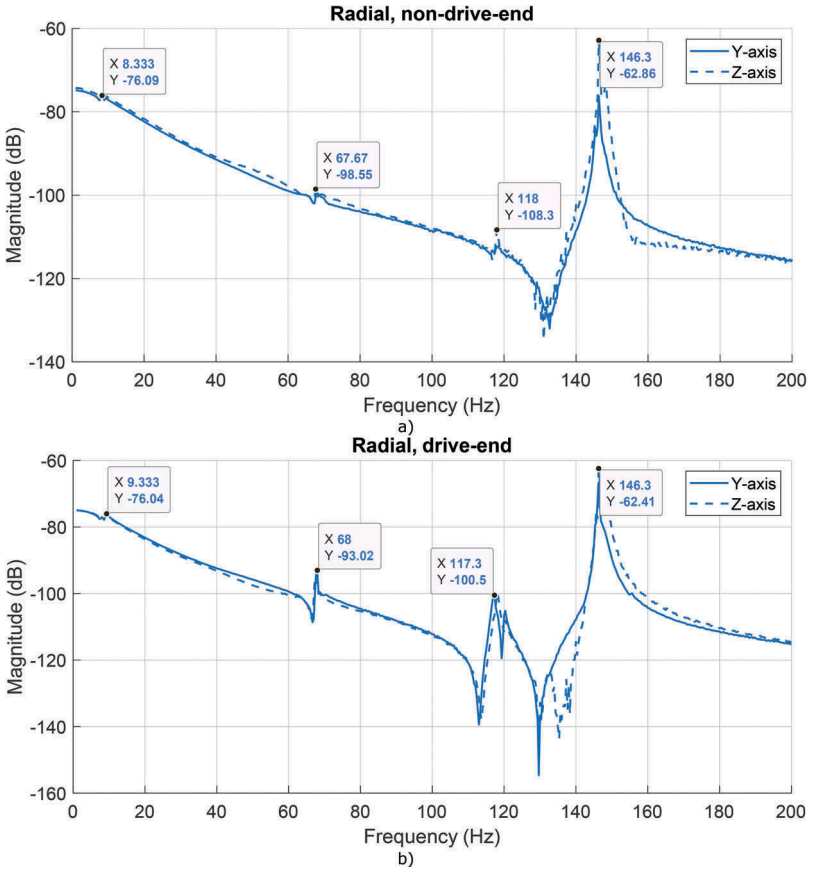


**Figure 4. Measured radial frequency responses: a) non-drive-end, and b) drive-end.**

### 4.2 Identification of eigenmodes

Previously identified resonance at the frequency of 117 Hz seemed to be happening at the both ends of the generator frame in both axial and radial directions. Thus, the solved undamped eigenmodes of the reduced-order model were investigated and the identified mode based on the description derived based on the measured data is visualized in Figure 5. As seen in the figure, both bearing end plates are deforming in the axial direction. In addition, the upper bearing end plate seems to be bending non-symmetrically as illustrated with the red dashed line in the Figure 5. This non-symmetric bending provides proof for the axial-radial coupled vibration seen in the measured sensor data.

Reason for the non-symmetric upper bearing end plate bending seems to be due to the power cable inlet located on one side of the upper bearing end plate, as seen in Figure 2. Further investigations revealed that the total deformation of the axial frame mode at 117 Hz is not centralized only to the bearing end plates, but, in fact, the whole frame tube was compressing and expanding in axial direction.

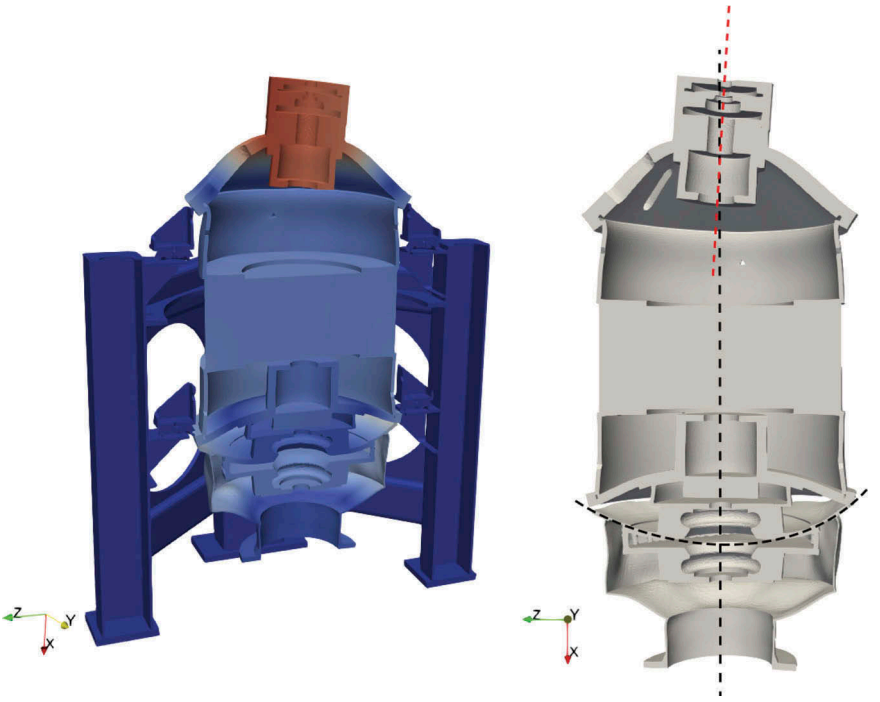


**Figure 5. Identified frame vibration mode of the resonance at 117 Hz. On the left is the mode visualization of complete assembly using great deformation factor, and on the right is the visualization of the skewed local bending of the upper bearing end plate.**

The relevant resonance peaks were identified from the measured sensor frequency response with the numerical model. Even though, the accuracy of the solved eigenfrequencies was not perfect due to many simplifications in the geometry, the measured eigenfrequencies were able to be matched to the corresponding simulated mode shapes. These relevant mode shapes were selected for harmonic analysis. The corresponding eigenfrequencies were updated to the modal coordinate model based on the measured sensor frequency responses. Further reduced modal coordinate expression was utilized for purposes of updating the exact modal damping ratios based on the measured data. Calculated damping ratios are presented in Table 2. The original model having 2,725,005 dofs is reduced to 1,632 dofs in superelement-based model and then further reduced to modal coordinate model having only 7 dofs. This drastic reduction could be performed without noticeable loss of accuracy compared to the full-sized problem. The accuracy of Craig-Bampton method based superelement expression, in general, is dependent on the number of selected modes for the transformation, while a good choice of the boundary degrees-of-freedom is also important. In addition, the reduced 7 dof modal coordinate model can be easily expanded back into the original full model with over 2.7 Mdofs, as presented in Section 2.3.

In Figure 6 are plotted the relative axial and radial frequency responses at the axial and D-end radial bearing sensor locations simulating the real measuring conditions. As theorized, the problematic frame vibration mode at 117 Hz is, indeed, visible on both axial and radial relative frequency responses. The other identified modes are described in Table 2. By comparing the measured and simulated response amplitudes, the following can be concluded:

- Frame rigid axial mode is barely visible in the simulated response due to large modal damping, the frequency of resonance peak of this mode seems to be a bit lower than in measured case as seen in Table 2.
- Steam outlet pipe axial mode is also in both measured and simulated radial responses. Although, the radial steam outlet pipe response is not visible in the simulated radial response.
- The problematic frame vibration at frequency of 117 Hz is visible in both axial and radial directions in the simulated response as well, and thus, proofing the existence of global coupled axial-radial vibration mode. Naturally, this mode is mainly axial as seen by comparing the magnitudes in Figure 6.
- Highly damped second axial frame mode at 205 Hz is lower in magnitude than in the measured response.

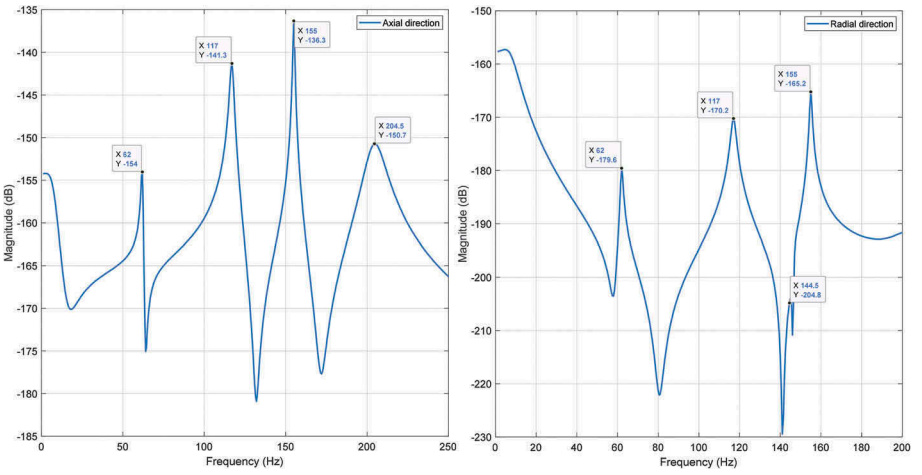


**Figure 6. Simulated relative responses at sensor locations: on the left is the upper axial sensor frequency response, and on the right is the D-end radial sensor frequency response.**

**Table 2. The identified eigenmodes based on the numerical model.**

| Measured frequency | Calculated damping ratio | Direction | Location | Mode shape |
|---|---|---|---|---|
| 8.5 Hz | 58.82% | Axial | Frame global | Rigid axial |
| 62 Hz | 0.97% | Axial | Steam outlet pipe | Umbrella |
| 68 Hz | 0.66% | Radial | Steam outlet pipe | Bending |
| 117 Hz | 1.07% | Axial/ Radial | Frame global | 1. axial mode |
| 146 Hz | 0.24% | Radial | Rotor | 1. lateral bending |
| 155 Hz | 0.34% | Axial | Rotor | Rigid axial |
| 205 Hz | 3.18% | Axial | Frame global | 2. axial mode |

## 5 CONCLUSIONS

Model-order reduction, solution expansion and Craig-Bampton transformation-based reduced-order model update for large structural dynamic problems is discussed. As a case example, 1MW steam generator frame dynamics is studied. The generator model is divided into three submodels, and superelements are generated from every submodel. Measured frequency responses from different AMB sensor locations indicated large vibration amplitude at 117 Hz in different directions between the sensor and rotor. Using superelement-based reduced-order model, the unknown frame vibration mode was identified by means of expanding the reduced-order solution in order to visualize the vibration mode using full-sized model. Once the problematic and other relevant vibration modes were identified by expanding the solved eigenvectors of Craig-Bampton transformation-based assembled superelement model, the reduced-order model was updated based on measured frequency responses. The measured mode frequencies and modal damping ratios were updated into the numerical model, and simulated model-based harmonic responses were calculated. These simulated frequency responses indicated the proof for the existence of axial-radial coupled vibration mode of the generator frame.

## REFERENCES


[1] Schweitzer, G., Maslen, E.H., "Magnetic Bearings", *Springer*, 2009.

[2] Blades, E.L., Craig, Jr., R.R., "A Craig-Bampton Test-Analysis Model", *Proceedings of SPIE - The International Society for Optical Engineering*, 1997, pp. 1386–1391.

[3] Seshu, P., "Substructuring and Component Mode Synthesis", Journal of Shock and Vibration, 4 (3), 1997, pp. 199–210.

[4] Boo, S.-H., Kim, J.-H., Lee, P.-S., "Towards improving the enhanced Craig-Bampton method", *An International Journal of Computers & Structures*, 196, 2018, pp. 63–75.

[5] Qu, Z.-Q., "Model Order Reduction Techniques with Applications in Finite Element Analysis", *Springer*, 2004.
[6] Wijker, J.J., "Mechanical Vibrations in Spacecraft Design", *Springer*, 2004.
[7] Friswell, M.I., Garvey, S.D., Penny, J.E.T., "Model reduction using dynamic and iterated IRS techniques", *Journal of Sound and Vibration*, 186(2), 1995, pp. 311–323.
[8] ANSYS, Inc. ANSYS Mechanical APDL Theory Reference. *ANSYS, Inc*., 2013.
[9] Sikanen, E., "Dynamic analysis of rotating systems including contact and thermal-induced effects," Doctoral Dissertation, *LUT University*, 2018.
[10] Lalanne, M., Ferraris, G., "Rotordynamics Prediction in Engineering", *John Wiley & Sons*, 1998.